Outcomes of the collapse of a large bubble in water at high ambient pressures

Jonathan R. Sukovich,[1,*] Phillip A. Anderson,[1] Ashwinkumar Sampathkumar,[1] D. Felipe Gaitan,[2] Yuri A. Pishchalnikov,[2,†] and R. Glynn Holt[1,‡]

[1]*Department of Mechanical Engineering, Boston University, Boston, Massachusetts 02215, USA*

[2]*Impulse Devices, Inc., Grass Valley, California 95945, USA*

(Received 30 December 2016; published 4 April 2017)

Presented here are observations of the outcomes of the collapses of large single bubbles in H_2O and D_2O at high ambient pressures. Experiments were carried out in a high-pressure spherical resonator at ambient pressures of up to 30 MPa and acoustic pressures up to 35 MPa. Monitoring of the collapse events and their outcomes was accomplished using multiframe high-speed photography. Among the observations to be presented are the temporal and spatial evolution of light emissions produced by the collapse events, which were observed to last on the order of 30 ns and have time independent radii on the order of 30 μm; the production of Rayleigh-Taylor jets which were observed to travel distances of up to 70 μm at speeds in excess of 4500 m/s; the entrainment of the light emitting regions in the jets' remnants; the production of spheroidal objects around the collapse points of the bubbles, far from any surface of the resonator; and the traversal and emergence of the Rayleigh-Taylor jets through the spherical objects. These spheroidal objects appear to behave as amorphous solids and form at locations where hydrodynamics predicts pressures in excess of the known transition pressures of water into the high-pressure crystalline ices, Ice-VI and Ice-VII.

DOI: 10.1103/PhysRevE.95.043101

I. INTRODUCTION

Bubble collapse phenomena have been studied extensively in recent years owing to the often violent effects of strongly collapsing bubbles. Single bubble sonoluminescence (SBSL), the process by which a light emitting gas bubble is trapped in a resonant sound field, has been a topic of great interest since it was first observed by Gaitan *et al.* [1]. Simulations of, and experiments with, the highest energy collapses have suggested that temperatures and pressures inside the collapsing bubbles may be in excess of 100 000 K and 150 GPa, respectively [2–5]. To that end, the size and duration of SBSL events have been studied rigorously to provide physical constraints on the processes involved in producing the observed light emissions. Previous studies of SBSL events, carried out in acoustic resonators operating at ambient or minimally over pressured static pressures, have shown that light emissions typically last on the order of 30 to 300 ps [6], and that the emitting regions typically have diameters on the order of 3 μm [7] or less. Recent work by Ramsey and Pitz [8] studying single-shot emission events produced by the collapse of large single bubbles (R_{max}=1.8 mm) in an unpressurized environment have shown light emitting regions with radii on the order of 28 μm and which last on the order of 15 ns. Recent work studying the emission events produced by the collapse of large bubble clouds in highly over-pressured environments (up to P_∞=30 MPa), has shown light emitting regions with radii as large as 500 μm and lifetimes of up to 70 ns [3].

In addition to the high temperatures and pressures reached within collapsing bubbles, however (and as Lord Rayleigh and the British admiralty recognized a century ago [9]), the pressure in the liquid outside a collapsing bubble can be predicted to reach upwards of 100 GPa in a few tens to hundreds of nanoseconds, with an associated rise in temperature of only a few degrees assuming adiabatic compression [10]. These temperatures and pressures are consistent with the formation of a number of high-pressure crystalline phases of water ice [11]. Indeed, the possibility of the transient formation of high-pressure forms of ice was suggested by Flynn as early as 1957 [12], and later theoretically predicted by Hickling [13] as a way to explain some of the anomalous features of sonoluminescence. However, in the absence of a surface on which crystal nucleation sites may form, the time scales involved in the pressurization process and the associated fluid dynamics in the high-pressure regions surrounding collapsing bubbles are not conducive to a crystalline transition [14]. That stable, moderately oscillating bubbles may nucleate dendritic growth of crystalline ice in undercooled water was shown by Ohsaka and Trinh [15], while Lindinger *et al.* [16] demonstrated that transient laser-induced optical breakdown and bubble collapse efficiently nucleated crystallization of undercooled water. In fact, cavitation-aided freezing and crystallization of either undercooled or supersaturated liquids is widely utilized [17].

In addition to the crystalline phases of water ice, a number of amorphous phases of ice also exist [18], and they are thought to be very likely the predominant form of the water found throughout the universe [19–22]. While these phases have only been observed to form at or near cryogenic temperatures [23–25], they possess a number of interesting characteristics relevant to this study. Particularly, the low-density amorphous (LDA) and very-high-density amorphous (vHDA) types have been shown to exhibit properties of ultraviscous liquids with viscosities up to 15 orders of magnitude greater than normal water [26]. Moreover, the pressures at which these phases form, between 0.2 and

*Present address: Department of Biomedical Engineering, University of Michigan, Ann Arbor, Michigan 48105, USA; jsukes@bu.edu

†Present address: Burst Laboratories, Inc., 13346 Grass Valley Ave, Grass Valley, CA 95945, USA.

‡rgholt@bu.edu

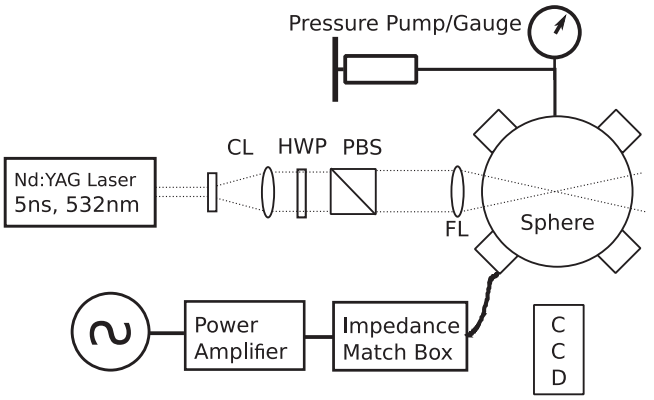

FIG. 1. Schematic of the experimental setup. CL, collimation lenses used to expand beam waist from 1 to 25 mm. HWP, half wave plate used to adjust the polarization angle of the light exiting the laser. PBS, polarizing beam splitter used in combination with the half wave plate to adjust downstream laser energy. FL, 125-mm focal length lens used to focus laser into the center of the spherical resonator.

1 GPa [27], are well within the range of pressures predicted in the vicinity of collapsing bubbles as we show below.

In this paper we present time-resolved images of the phenomena associated with and produced by the collapse of large single bubbles in a highly over-pressured environment. Observations of the final stages of the bubbles' collapses, on through the evolution of events at the collapse point and in the surrounding fluid thereafter, have been made.

II. METHODS

A schematic drawing of the experimental setup used during this study is shown in Fig. 1. Bubbles in experiments were nucleated [28] using a pulsed Nd:YAG laser focused into the center of a water-filled, high-pressure spherical resonator (Impulse Devices, Inc). Experiments were carried out in both H_2O and D_2O water at static pressures of up to 30 MPa. The resonator was driven at a frequency of 28 kHz, and at acoustic pressure amplitudes just below the cavitation threshold of the system, such that the absolute negative pressure reached by the acoustics, regardless of the static pressure, was maintained at approximately -5 MPa [29]. Water used in experiments was filtered to 0.2 μm and was degassed by equilibration with air at 16 kPa. Time resolved images of individual events were captured using a high-speed camera (SIM-X8, Specialised Imaging, UK) with 8 CCD elements whose exposure and interframe times were independently variable. Each eight-frame image series to be presented is associated with the nucleation of *one* single bubble and captures different aspects of the bubble's evolution, including its collapse and the events that develop in the fluid surrounding it thereafter. Images of the events captured were backlit using a white CW light source to allow for the simultaneous capture of the bubble dynamics during and following the collapse. For a more detailed description of the experimental setup and methodology see our previous paper [30].

III. RESULTS

We first remark on the appearance and development of diffuse dark bands around the collapsing bubbles (Figs. 3–5, 8, and 9). These diffuse dark regions may be attributed to the shape and magnitude of the pressure field built up in the fluid surrounding the collapse point of the bubble (described by Lord Rayleigh in [9]) and water's pressure-dependent index of refraction [31], which combine to create gradients in the local index of refraction in the water around the collapsing bubble that extend radially outwards from it, and which act to refract incident light from the camera's backlight source out of the region being imaged. As the size of the bubble decreases during the course of its collapse, the magnitude of the refractive gradients in the field around it grow and cause the dark region around the bubble to appear to become darker and grow in extent as the amount of light refracted out of the region increases continuously until the collapse is arrested. Following collapse, these dark regions are observed to travel outward from the collapse point, eventually becoming the well-studied shock waves associated with collapsing bubbles [32], and the pressure fields and refractive gradients around the collapse point renormalize to restore an unobstructed view of the field.

As the diffuse dark regions traveled outward, however, ringlike, spheroidal structures were observed to have formed in the areas obscured by their presence in the fluid region surrounding the collapse points of the bubbles (Figs. 4, 5, 8, and 9). These ringlike objects were consistently observed to have formed in the fluid following the bubbles' collapses and were observed to remain nearly stationary in the fluid until disturbed by the growth of bubbles in the region in later acoustic cycles (Figs. 10 and 11). One important feature of these objects particularly germane to the following discussions is that their radii were observed to be linearly proportional to the maximum radii of the bubbles that generated them. Owing to the eight-frame limit imposed by the camera used to capture these events during experiments, this relationship was used as a proxy for direct measurements of the bubble's maximum radius where necessary when this measurement was not directly available in images. These ringlike structures will be described in more detail later.

A. Macroscopic spherical collapse parameters

Images were captured during experiments which sought to capture the dynamics of the generated bubbles during and after their collapses. Among the macroscopic features captured were the radii of the bubbles as a function of time during their collapses, the production of high-velocity Rayleigh-Taylor jets following, and the emissions of shock waves thereafter. Multiple series of images showing these and other phenomena may be seen in Figs. 3–5 and 8–11. The maximum radii of bubbles generated during these experiments ranged from approximately 0.8 to 1.8 mm.

Analysis of the dynamics of the bubbles during their collapses revealed a number of notable features. First, collapse events were often observed to produce bubble wall velocities in excess of 3000 m/s, with the most energetic collapses producing bubble wall velocities in excess of 7000 m/s near their collapse points (Fig. 2). The minimum observed

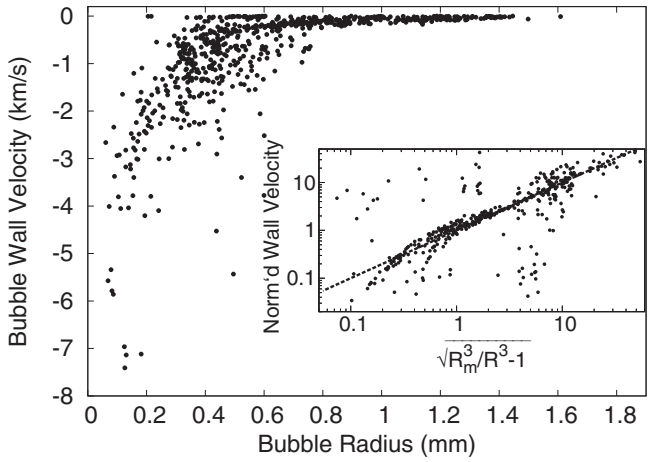

FIG. 2. Bubble wall velocity vs bubble radius for single cavitation bubbles (H_2O and D_2O data combined). The inset plot shows that the bubble wall velocity (normalized by $\sqrt{2P_\infty/3\rho}$) was linearly proportional to the quantity $\sqrt{R_m^3/R^3-1}$, where P_∞ is the static pressure, ρ is the density of the species of water used, and R_m and R are the bubble's maximum and instantaneous radii, respectively. The dotted line in the inset plot shows the theoretical relationship between these two quantities from Eq. (1).

radii of the bubbles studied during these experiments were seen to be on the order of 50 to 100 μm, however, as the formation of the diffuse dark regions described above often obscured the view of bubbles with potentially smaller radii, measurements of smaller bubbles could not be made. Collapse events were largely observed to follow the dynamics predicted by Rayleigh [9], even as they approached the ends of their collapses. Particularly, the relationship of the bubble wall velocity to its instantaneous radius was observed to follow the scaling relationship given in Eq. (1),

$$\dot{R} = \sqrt{\frac{2P_\infty}{3\rho}}\left(\frac{R_m^3}{R^3}-1\right)^{1/2}, \tag{1}$$

where $\dot{R}$ is the bubble wall velocity, P_∞ is the ambient pressure of the fluid, ρ is the density of the fluid, and R_m and R are the bubble's maximum and instantaneous radii, respectively. As may be seen in the inset plot of Fig. 2, which shows the normalized bubble wall velocity versus the ratio of the bubbles' maximum radius to its instantaneous radius, there is good agreement between theoretical predictions and measured values. As noted above, where direct measurements of the maximum radii of the bubbles were not available, proxy values from measurements of the ringlike objects were used instead.

Rayleigh-Taylor jets were also often observed to be produced following the collapse of the bubbles generated during these experiments and exhibited a number of surprising characteristics and behaviors. First, jet tips in these studies were often observed to reach peak velocities in excess of 3000 m/s, with some of the fastest jets reaching apparent velocities of more than twice that. While these numbers are notable in their own right, owing to the unrestricted direction of travel of these jets and their unknown orientations with respect to the imaging plane of the camera, what we observe is actually a 2D projection of the jets' 3D motions, and so these numbers only represent *lower* bounds of the jets' actual peak velocities. As the direction of jets varied from shot to shot, however, and was not experimentally controllable, it was not possible to capture the jets lying consistently in the image plane to refine this measurement. Perhaps most surprising among the observations of these jets, however, was the entrainment within their tips of the light emitting regions described in the next section. This phenomenon is best illustrated in Fig. 5, where the light-emitting region can be seen traveling leftward in the image entrained in the jet tip. Interestingly, features of these jets including the development of toroidal vortices near the collapse points of the bubbles (Figs. 10 and 11), and the trajectories of the jets themselves (Fig. 9), were often observed to be influenced by or "preserved" within the spheroidal objects mentioned above. These features of the jets will be described in more detail below in the section dedicated to the production of these spheroidal objects.

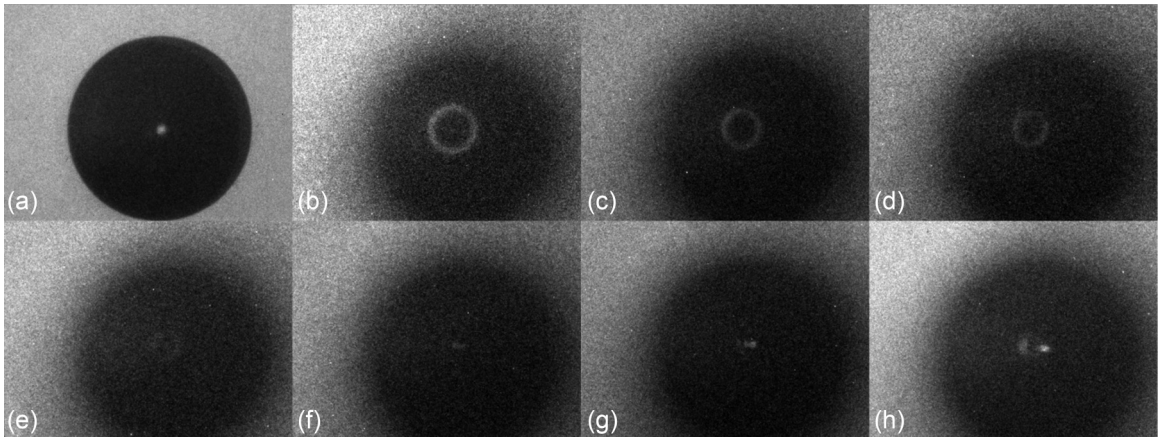

FIG. 3. Experimental details: frame dimensions = 1.75 × 1.32 mm; frame exposure times = 5 ns; P_∞= 17.2 MPa. The gap between frames in Frames (b) and (h) was 0 ns, giving an effective frame rate of 200 Mfps. This image shows the final stages of a bubble's collapse [frames (b)–(e)], followed by the generation of a light emitting region therein [frames (f)–(h)]. Frame (a) was captured 16 μs prior to frame (b) to ensure that the event observed was from a single bubble collapse.

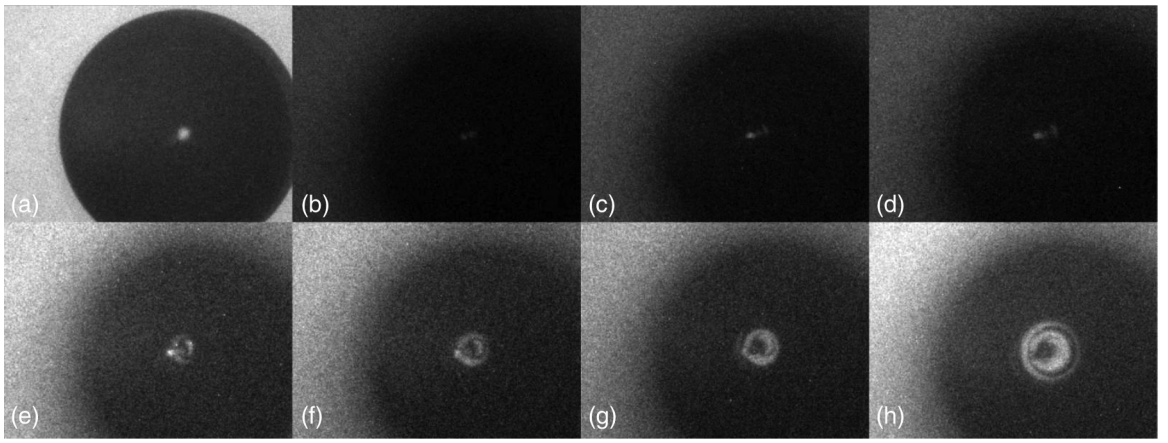

FIG. 4. Experimental details: frame dimensions = 1.75 × 1.32 mm; frame exposure times = 5 ns; P_∞ = 17.2 MPa. The gap between frames in frames (b) and (h) was 0 ns, giving an effective frame rate of 200 Mfps. This image shows the early development and time evolution of a light emitting region in frames (b)–(g). The light emitting region in frames (b)–(g) is observed moving leftwards from its point of origin during its lifetime. Starting in frame (e) and progressing through frame (h) we see the thick, dark band surrounding the light-emitting region traveling radially outwards from the center. In frame (h) we see a ringlike structure revealed in the light region encircled by the thick, dark band as it crosses over it. Frame (a) was captured 16 μs prior to frame (b) to ensure that the event observed was from a single bubble collapse.

Following the collapse of the bubbles, shockwaves were observed to develop and travel away from the collapse point. As noted above, the development of the high pressures in the fluid regions surrounding the collapsing bubbles, which eventually become the outgoing shockwaves, could be monitored prior to and during the collapse of the bubbles in the form of the development of the diffuse dark regions. Velocities of the outgoing shockwaves were measured to reach up to approximately 5000 m/s and were seen to remain supersonic out to a radius of about 300 μm.

B. Light emissions

Images of light emission events were captured which attempted to show the time evolution of emission events from their formation to their decay. However, the collapse times of the laser-nucleated bubbles exhibited a sufficient degree of inherent variability that it was not possible to reliably determine the exact moment of each bubble's collapse beforehand and gate the camera's acquisition accordingly. This collapse-time variability was likely due to small differences in the sizes of the generated bubbles, presumably due to variabilities in energy deposited into the generated cavitation nuclei by the laser beam and/or to small variations in the phase and amplitude of the acoustic pressure at the moment of nucleation. Owing to the eight-frame limitation of the camera, and the 5-ns exposures used to acquire images in the series (corresponding to a total time span of 40 ns), this inevitably caused the collapse events, and hence emissions, to occur at different times with respect to the camera's acquisition window, and as such most images of the light emissions showed only portions of the light-emitting region's

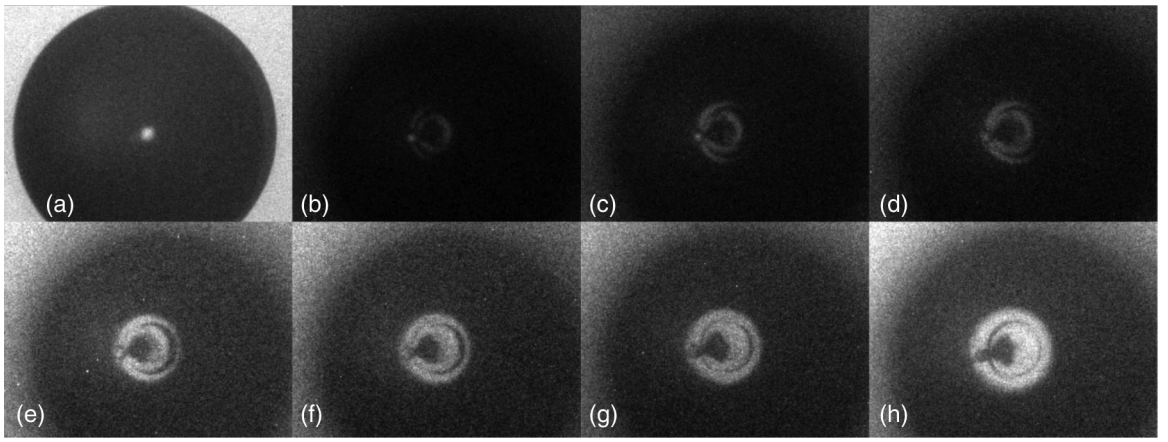

FIG. 5. Experimental details: frame dimensions = 1.75 × 1.32 mm; frame exposure times = 5 ns; P_∞ = 17.2 MPa. The gap between frames in frames (b)–(h) was 0 ns, giving an effective frame rate of 200 Mfps. This image shows the time evolution of a light emitting region near the end of its life [frames (b)–(e) and (f)] and what remains in the fluid region after emissions have ceased [frames (f)–(h)]. During its lifetime the light-emitting region is observed to travel leftwards, entrained in what is revealed in frame (h) to be a Rayleigh-Taylor jet remnant. In frames (b)–(h) a ringlike structure is observed in the form of the thin, dark band in the light region encircled by the thick, dark band traveling outwards from the center. Frame (a) was captured 16 μs prior to frame (b) to ensure that the event observed was from a single bubble collapse.

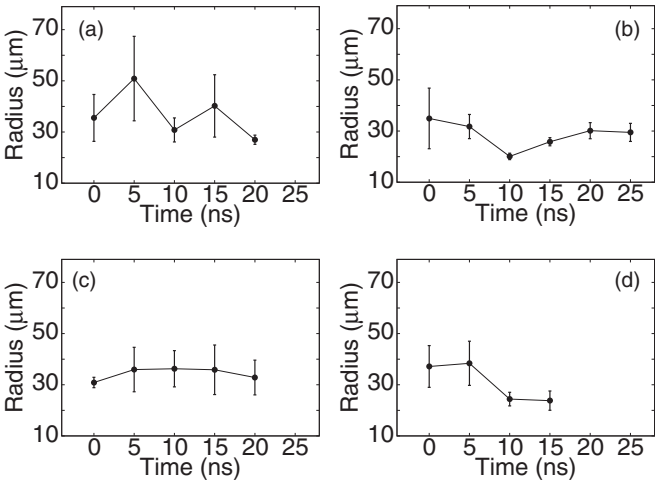

FIG. 6. Radius vs time plots of typical light emission events produced during collapses in H_20 at ambient pressures of 17.2 MPa.

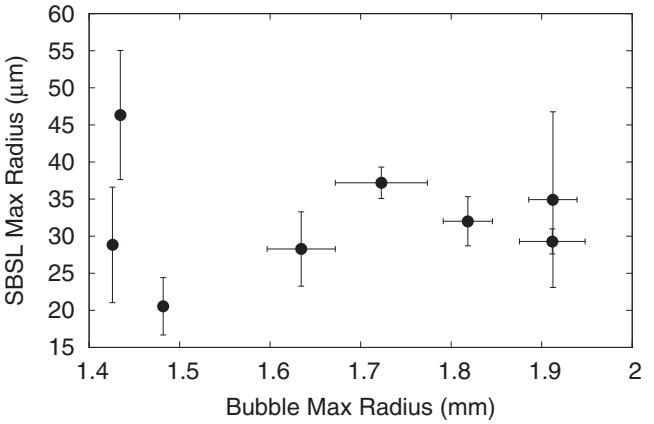

FIG. 7. This plot shows the maximum radius of the light-emitting region versus the maximum radius of the bubble that generated it.

evolutions. Three such images of emission events, generated by the collapses of bubbles nucleated under otherwise equivalent conditions, and which show the onset, evolution, and decay of these regions may be seen in Figs. 3, 4, and 5, respectively.

Images of the light emissions captured revealed a number of interesting features. First, as may be seen in Figs. 3(f)–3(h) and 4(b)–4(e), emissions are observed to be initially faint before growing brighter in the first 10 to 15 ns of their lifetimes. After reaching their peak intensities, emissions are observed to fade out over similar time scales as may be seen in Figs. 4(e)–4(g) and 5(b)–5(e). Combining the results of these images series we find the emission lifetimes of these events to be on the order of 20 to 30 ns. This is most readily apparent in Figs. 4(b)–4(g), which show an emission event over the greatest portion of its lifetime. These results are in good agreement with the recent results of Ramsey and Pitz [8], which show the lifetimes of emission events produced by the collapse of similarly sized bubbles in an unpressurized environment to be on the order of 15 ns. Interestingly, the lifetimes of the emission events observed in the present study are of the same order as those produced by the collapse of larger compact bubble clouds (∼70 ns) under similar ambient pressure and water preparation conditions [3].

The spatial evolution of emission events yielded further notable and surprising features. First, as may be seen in Figs. 6(a)–6(d), the radii of events observed were found to be on the order of 30 μm. These results are, again, in good agreement with the results of Ramsey and Pitz [8]. Interestingly, however, the radii of events observed showed no discernible growth or decay over the course of their lifetimes. This observation lies counter to observations of emissions produced by the collapse of compact bubble clouds, which showed emitting regions to grow explosively to radii of ∼300 μm before slowly shrinking away [3]. Some light-emitting regions were also observed to become entrained in Rayleigh-Taylor jet remnants generated as a result of instabilities during the final stages of the bubbles' collapses. While entrained, the light-emitting regions were observed to travel at the tip of the jet remnant until they were extinguished, up to 70 μm from their points of origin and at speeds in excess of 4500 m/s. This behavior is especially apparent in Fig. 5, where the light-emitting region can be seen traveling progressively leftward across the ring structure entrained in the tip of a jet remnant. It should be noted again, however, that these images only show a 2D projection of the jet's 3D motion and that, because the angle of the jet with respect to the image plane is unknown, measurements of the speed and distance traveled correspond only to lower bounds.

Further observations yielded an unexpected relationship between the maximum radii of the light-emitting regions and the maximum radii of the bubbles producing them which, to the best of the authors' knowledge, has not been described before. One might reasonably expect larger bubbles to produce more energetic collapse events and that this in turn would produce measurable differences in the sizes of the light-emitting regions generated. As may be seen in Fig. 7, however, this was not observed to be the case. Instead, the maximum radii of the light-emitting regions produced seem to be independent of the maximum radii of the bubbles that produced them. While this result may be a consequence of the limited number of events where information on both sets of radii could be obtained at once, or that, as noted earlier, where direct measurements of the maximum bubble radii were unavailable, they were estimated using the relationship between the radii of the ring structures and the bubbles that generated them (expressed in the comparatively large error bars for bubbles with maximum radii greater than ∼ 1.5 mm in Fig. 7), it bears remarking that the light emissions observed from the collapses of even the smallest bubbles described in the present study were seen to have radii nearly identical to those described in Ramsey and Pitz, despite having collapse energies nearly two orders of magnitude greater. This suggests that beyond a certain point the radii of the emission events may be only weakly dependent on, or independent of, the collapse energy and, by proxy, the maximum radii of the bubbles which generate them.

C. Spheroid production

In a typical experiment, optical breakdown is used to nucleate a small bubble in the center of a high-pressure spherical resonator [28], far away from any surfaces, which

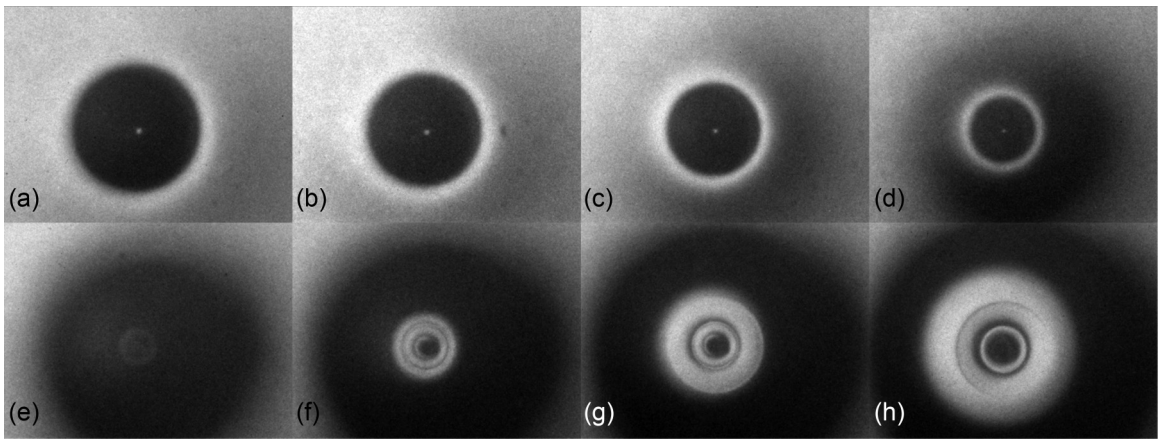

FIG. 8. Experimental details: frame dimensions = 1.75 × 1.32 mm; P_∞ = 17.2 MPa in H_2O. Successive images of a collapsing bubble [(a)–(e)] and the aftermath [(f)–(h)] during the first acoustic cycle after nucleation. Each frame had an exposure time of 20 ns with a 30-ns gap in between frames, resulting in an effective framing rate of 20 Mfps. The dark region around the bubble before and after the collapse is due to the high pressure in the liquid bending light away from the camera. Note the persistent ring-like structures in frames (f)–(h).

then grows into a macroscopic bubble during the tensile phase of the pressure field. During a typical collapse, the bubble implodes with supersonic velocity [Figs. 8(a)–8(e)]. The pressure in the liquid immediately outside the bubble [described by Eq. (2) below] gets so high that it refracts light away, resulting in the apparent diffuse dark region outside the collapsing bubble [Figs. 8(c)–8(h)]. By Fig. 8(h) the diffuse high-pressure region begins to travel away from the bubble and will become the well-studied shock wave emitted by a collapsing bubble [32]. This departing nascent shock reveals what appear to be concentric rings as seen in the central region of Fig. 8(h). It should be noted that this dark region is only evident very briefly near the end of a bubble's collapse, when the Rayleigh pressure in the field is at its highest. As such, the dark region is not apparent in images captured during the bubble's growth or early stages of its collapse, nor after the resultant shock waves have exited the field of view. This is the case in Figs. 10 and 11, where image acquisition was not timed to coincide with the bubble's collapse, and thus no dark bands are apparent.

As Figs. 9(e)–9(h), 10(a), and 10(b) show, the outer ring is apparently the boundary of a spheroidal object. This spheroidal object refracts light and so possesses a slightly different index of refraction than water. Comparing Figs. 8(h), 9(e), and 10(a), which appear to be three different views of the same object rotated through 90 degrees at different points in its lifetime, allows the inference that the apparent inner ring of Fig. 8(h) may be the outer boundary of a toroidal vortex. By again comparing the same three rotated figure frames, the central dark blob in Fig. 8(h) is apparently the remnant of a Rayleigh-Taylor jet [33], "frozen" within the spheroidal object and emerging into the liquid in a turbulent plume as seen in Figs. 9(d)–9(h) and 10. The presence of these jet remnants, or lack thereof, had no appreciable affect on the spheroid size with respect to the bubble maximum radius.

The behavior of these spheroidal objects, and their interactions with the media around them, are strongly suggestive of a phase transition in the liquid. The spheroids were observed to persist for upwards of 70 μs in the fluid, surviving at least a few acoustic cycles after forming. The size of the spheroids

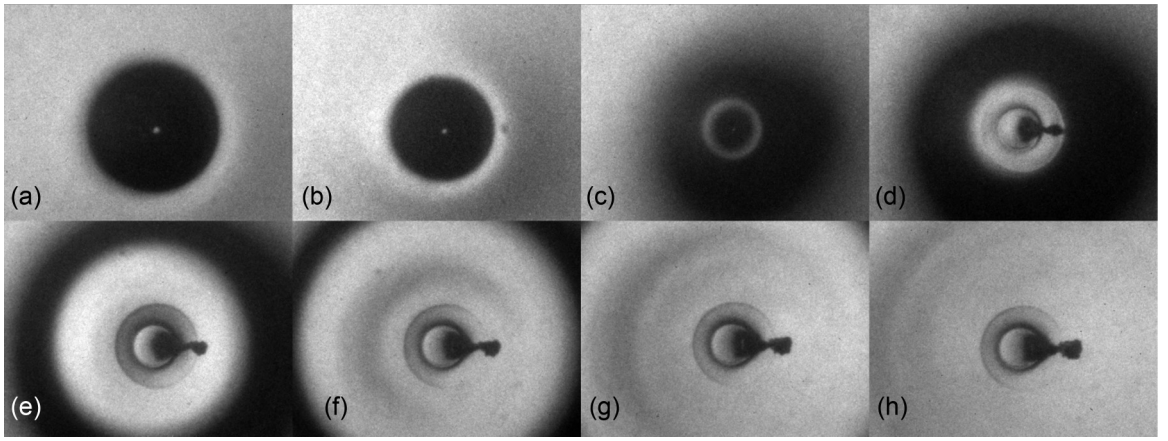

FIG. 9. Experimental details: frame dimensions = 1.75 × 1.32 mm; P_∞ = 17.2 MPa in H_2O. Successive images of a collapsing bubble [(a)–(c)] and the aftermath [(d)–(h)] during the first acoustic cycle after nucleation. Each frame had an exposure time of 20 ns with a 100-ns gap in between frames, resulting in an effective framing rate of 8.33 Mfps. The remnants of a Rayleigh-Taylor jet are visible in frames (d)–(h).

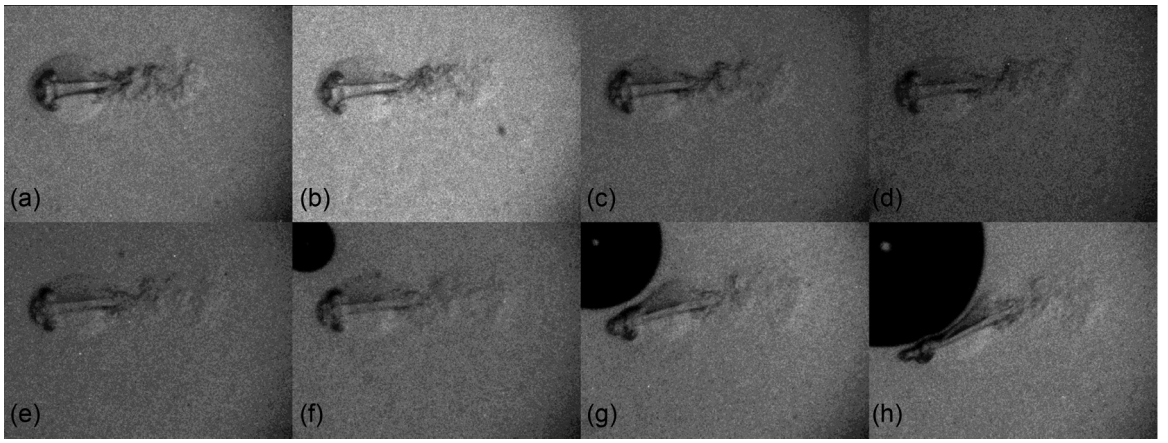

FIG. 10. Experimental details: frame dimensions = 1.75 × 1.32 mm; P_∞= 20.7 MPa in D_2O. Evolution of spheroid with a frozen remnant jet and toroidal vortex during the second acoustic cycle following nucleation. Frames (a)–(d) had an exposure time of 5 ns, (e)–(h) had increasing exposure times of 10–60 ns, with a 2.5-μs gap in between frames, resulting in an effective framing rate of 400 kfps.

was observed to slowly shrink at a rate of roughly 0.33 m/s; however, the eventual radial decay of the spheroids was not observed, and they were instead only seen to be torn apart by bubble activity in their vicinity in subsequent acoustic cycles. Many spheroids were observed to withstand the bombardment from expanding and collapsing bubbles in the later acoustic cycles after their initial appearance, with some subsequent collapse events even resulting in the production of another spheroid in the field (Fig. 11).

Perhaps more dramatic than the longevity of these objects is their apparent deformability. In Fig. 11 we observe the spheroid being deformed by the expansion of a secondary bubble; upon the collapse of the secondary bubble, the original spheroid has regained its initial shape. In Fig. 10 we see a spheroid with a "frozen" remnant jet and toroidal vortex slowly deform under the influence of the motion of the jet remnants [Figs. 10(a)–10(e)], until a new bubble expands and deforms the spheroid more rapidly [Figs. 10(f)–10(h)].

Rayleigh-Taylor jet remnants are observed to travel through the structures as may be seen in Figs. 9 and 10. The very existence of a jet upon the first collapse of a bubble far from boundaries is interesting in its own right; however, its motion through the spheroid is indicative of a change in transport properties across the boundary of the object. The jet is noticeably altered when it first reaches the boundary of the spheroid, appearing to bend out of line upon contact [Figs. 9(d)–9(e)]. Upon passing the boundary of the spheroid, the emergent portion of the jet appears to grow rapidly outwards, while the portion entrained within the spheroid appears to change at a much slower rate [Figs. 9(e)–9(h)]. This is especially apparent at later times after the jet has fully emerged, as seen in Fig. 10. The jet seems to have traveled through the structure along a relatively smooth path and upon reaching the outer wall, "blossomed" outwards and left ejected material (and/or turbulent fluctuations) in its wake. The change in jet behavior associated with its interaction with the wall implies a dramatic change in transport properties across the boundary.

Toroidal vortices, as seen in Fig. 10, are often observed as the result of an asymmetric jetting bubble collapse [34,35]. The toroidal vortices observed indicate that the jet moved through the already formed spheroidal object, creating the vortex as

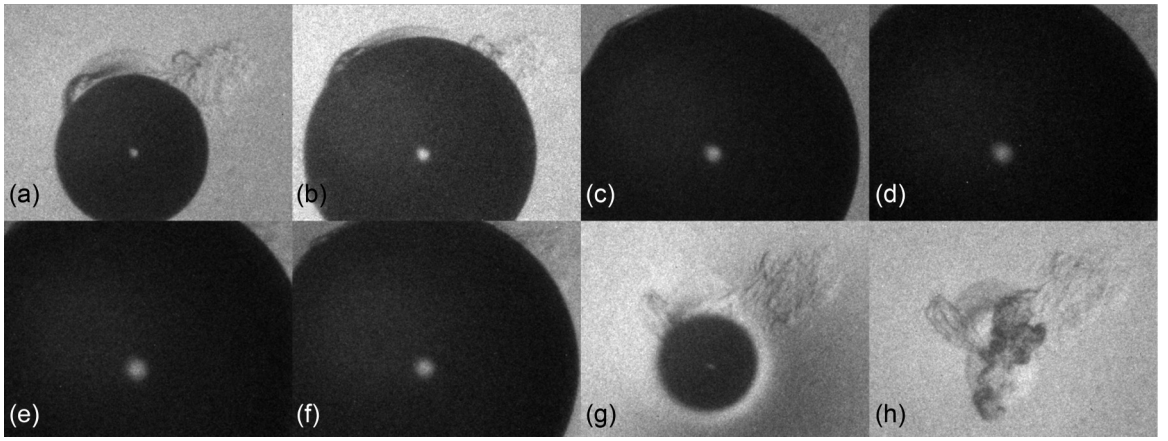

FIG. 11. Experimental details: frame dimensions = 1.75 × 1.32 mm; P_∞ = 20.7 MPa in D_2O. Deformation of an existing spheroid [upper left in frame (a)] by expanding bubble during the second acoustic cycle following nucleation. Frame timings are identical to those described in the caption of Fig. 10. The collapse of the bubble creates a second spheroidal object visible in frame (h).

it passed through and implying either that the spheroid has a different viscosity than water, or that it was locally 'melted' by the passage of the jet.

Further evidence of altered transport properties of the spheroids may be found by examining the nucleation and growth of bubbles near the objects in later acoustic cycles. Particularly, as may be seen in Figs. 10(f) and 11(a), the nucleation sites of bubbles near the spheroids do not seem to be explicitly linked to locations where the undissolved gas remaining from the previous bubble's collapse might reasonably be expected, i.e., within the spheroid near the center point of the bubble's collapse, or near the emergent portion of the jet in the fluid surrounding the spheroid. While some bubbles spontaneously nucleated in later cycles were observed to grow in these regions, that they don't explicitly seems to suggest that the material that makes up the spheroids acts to effectively shield the region from the negative pressures that would otherwise cause bubble nuclei in the region to grow, or that the growth of nuclei in the region is suppressed in spite of reaching pressures requisite for growth. It may also be seen in Fig. 10(h) that the spheroid impinges upon the growth of the bubble near it. This is evident in the observed deformation of the bubble wall located near the top half of the toroidal vortex within the deformed spheroid. The ability of the spheroids to suppress the growth of nuclei in the region, and to impinge upon the growth of bubbles in later acoustic cycles, again suggests that the spheroids have different transport properties than bulk water.

IV. DISCUSSION

In this study we have observed a number of interesting and highly surprising features associated with the collapse of large single bubbles in a highly over-pressured environment, including the production of large, long-lived light emission events; high velocity Rayleigh-Taylor jet remnants; the entrainment of the light-emitting regions within said Rayleigh-Taylor jet remnants; and the production of previously undescribed spheroidal objects around the collapse points of the observed bubbles and their interactions with the other phenomena listed.

Observations of light emissions showed that they had lifetimes on the order of 20 to 30 ns and radii between about 25 and 40 μm. While these results are in good general agreement with the results of Ramsey and Pitz studying the collapse of similarly sized bubbles in an unpressurized environment [8] (where lifetimes and radii of emission events were observed to be approximately 15 ns and 28 μm, respectively), it is notable that the difference is not more pronounced. That is to say, because the experiments of this study were carried out in a highly over-pressured environment (up to 30 MPa), as opposed to at ambient pressures as in Ramsey and Pitz, the energy available to the collapse should have been to be up to two orders of magnitude or more greater owing to the effects on the collapse dynamics higher ambient pressures have, including significantly increasing both the bubble wall velocity [Eq. (1)] and the velocity of the inrushing fluid surrounding it [9]. While such large differences in collapse energies might reasonably have been expected to produce significant differences in either the sizes or durations of the emission events between these two studies, a number of potential factors may offer explanations as to why they did not.

First, the similarity in the sizes of the emitting regions may be the result of the similarity in sizes of the bubbles that generated them, wherein one might consider the size of the light-emitting region to be purely a function of the maximum radius of the bubble generating it. In such a model, light emissions might be regarded as a function of the volume compression ratio of the gases contained within the bubble upon reaching its maximum radius, after which point the bubble would collapse as a closed system whose motion would come to a halt as light emissions began. Under similar water preparation and nucleation conditions, the diffusion of mass into the bubbles during their growth phases would presumably lead to similar internal gas and vapor content, which would only be weakly dependent on the ambient pressure of the surrounding fluid. Using the results from experiments to empirically determine the threshold compression ratio for emissions (based on emission events generated in each experiment by bubbles with maximum radii of 1.8 mm), the compression ratio for emissions is found to be between approximately 1.5×10^5 and 2.5×10^5. Using the midpoint compression ratio of 2×10^5, this simplified model predicts that bubbles with maximum radii of 1.4 and 1.9 mm would produce light emitting regions with radii of 24 and 33 μm, respectively, which is in agreement with the sizes of the emitting regions observed in the present experiments.

If this model is correct, however, it still leaves the extra collapse energy unaccounted for. The lifetimes of the events measured in the current experiments were observed to be similar to those observed in Ramsey and Pitz, and ranged from approximately equal in duration to up to a factor of two greater. This increased lifetime may account for some of the extra energy and would seem to suggest the formation of a hotter plasma with a longer decay lifetime, or that the compression was sustained for a longer amount of time after emissions began, thus extending the emission lifetimes. As spectroscopic imagining of these events was not available during these studies, determination of the temperatures within the light-emitting region could not be made. However, the size of the emitting regions was not observed to have a functional dependence on time, which might be expected if compression of the volume continued.

In relation to the similarity between the results of the present experiments and those of reference [8], it has also been theoretically suggested that strength of a bubble's collapse can be nearly independent of the driving conditions for relatively high acoustic amplitudes [36–39]. In turn, it has been suggested that this can result in similar collapse strengths for bubbles over a wide range of the expansion ratio, R_{max}/R_0, and that the maximum temperatures reached within the collapsing bubbles can be nearly independent of the driving acoustic pressure amplitude [36–39]. The suggested reasons for these outcomes include cooling of the bubble interior due to the endothermic dissociation of trapped water vapor and the prediction of an upper bound for the bubble wall velocity during collapse [36–39]. However, the predicted upper bound in the collapse velocity is determined by the sound speed at the bubble wall, rather than the ambient sound speed of the fluid, and thus increases with the increasing

Rayleigh pressure produced during the bubble's collapse. Indeed, our experimental observations show that the bubble wall velocity scales as expected throughout the duration of its collapse (Fig. 2) even as it exceeds Mach 1 with respect to the ambient liquid conditions, and provide evidence that the Rayleigh pressure increases with R_{max}. As a laser was used to nucleate the bubbles in this study, no satisfactory definition of the "equilibrium radius", R_0, could be established to assess the effects of the expansion ratio, and the dependence of collapse outcomes on acoustic pressure amplitude was not investigated.

An alternative explanation for the similarity between the results of these two experiments may be found in the formation of the observed Rayleigh-Taylor jets and the entrainment of the light emitting regions within their tips. Particularly, that the energy of the collapse should be deposited primarily or wholly to the bubble's core is based on the notion that the collapse remains spherically symmetric throughout its duration. While light emission events were observed in the absence of any apparent jetting, this was demonstrably not the case during the majority of events captured, as is evident in the formation of strong jets following collapse, whose tip velocities in the lower bound were observed to reach in excess of 4500 m/s. It may be the case that the conditions under which emissions begin also represent the threshold beyond which inertial instabilities dominate the collapse process, leading to the formation of the observed jets and the siphoning off of energy from the field to drive their motion.

Observations of the entrainment of the light-emitting regions within the remnant jet tips might also provide an explanation for the apparent lack of time dependence on their sizes. Notably, the motions of the light emitting regions were observed to be subject to the flows of the materials within or surrounding them, as evidenced by the motion of the emitting region away from the collapse point in Fig. 5. A reasonable extension of this observation would be to say that in addition to bulk motion, the light emitting species within the jet tip would also be subject to smaller scale turbulent flows within the jet itself. This in turn could make the size of the emitting region a variable quantity, subject to the position from one moment to the next of the light emitters within.

Perhaps the most interesting explanation for the similarity between the results of these experiments and those of Ramsey and Pitz may be found in the formation of the observed spheroidal objects. As described earlier, the behavior of these objects and their interactions with the other observed phenomena suggest that they have different transport properties than the water surrounding them. If one assumes that the formation of these spheroids impedes the motion of the fluid driving the collapse, it can be shown that the difference in energy densities between the fluid regions encapsulated by the boundaries of these spheroids and the final collapse points of the largest and smallest experimentally observed bubbles in this study is less than 5% [40]. If the measurable quantities of the light emitting regions are dependent on the energy density of the unbound fluid surrounding them, the formation of the spheroidal objects could account for the observed result. One such process which could lead to a change in transport properties in the media, which would thus impede the inward motion of the fluid driving the collapse, is a phase transition in the water.

The conditions present in the fluid surrounding our collapsing bubbles are sufficient to produce a phase change in water as long as there is enough time for the phase transition to occur; other investigations [14] have shown that shock wave compression can trigger nucleation and dendritic crystal growth on a boundary in as little as 5 ns. The pressurization process examined in the present study, we stress, is not the result of shock wave compression and associated heating. Instead, high pressures in this study are reached as a result of continuous geometric contraction of the inrushing fluid region surrounding a bubble during the final stages of its collapse. To obtain useful bounding values of the pressures generated during this process, the pressure in the fluid around the bubble can be described in the incompressible limit by the Rayleigh equation [9],

$$P(r) = P_\infty\left[1 + \frac{R}{3r}\left(\frac{R_m^3}{R^3} - 4\right) + \frac{R^4}{3r^4}\left(1 - \frac{R_m^3}{R^3}\right)\right], \quad (2)$$

where P_∞ is the static ambient pressure in the fluid, R is the instantaneous radius of the bubble, r is the distance from the center to a point in the fluid, and R_m is the initial maximum radius of the bubble. As a reference, a collapsing bubble with a maximum radius of 1.5 mm and an instantaneous radius of 40 μm is predicted to produce a spatial peak fluid pressure in excess of 100 GPa.

If the pressurization process does produce a phase transition in the fluid, a reasonable assumption would be that the transition begins when the pressure in the liquid first exceeds some critical threshold value, P_t. It is then required to find the radial location where the peak pressure first exceeds that critical value. This can be accomplished by manipulating Eq. (2) to find the radial location, r_{peak}, of the peak pressure in the field which yields

$$r_{peak} \approx \frac{R_m}{1.16}\left[\frac{P_\infty}{P_{peak}}\right]^{1/3}, \quad (3)$$

where the approximation is taken in the limit of $P_{peak} \gg P_\infty$. This yields a linear relationship between the bubble's maximum radius and the radius of the assumed transition pressure in the liquid. A comparison between this relationship and the observed location of the inner and outer rings of the spheroids can be seen in Figs. 12(a) and 12(b), respectively. Allowing P_{peak} to be a (constant) fitting parameter, P_t, there is good agreement between theoretical predictions of the radius in the fluid where the peak pressure first reaches $P_t = 1.6$ and 18 GPa, and the experimentally observed outer and inner spheroid boundaries, respectively. Of course, the pressure at these radial locations continues to rise until the motion of the radius of the bubble wall, R, is halted at some minimum radius R_{min} by the buildup of the interior gas and/or vapor pressure in the bubble. Excluding times after the radius of the bubble reaches its minimum, R_{min}, the maximum pressure at any location, r, in the fluid would be given by Eq. 2 with $R = R_{min}$.

While the fluid pressures calculated at the locations of the rings (1.6 and 18 GPa) don't correspond exactly with known transition pressures for the crystalline phases of water ices, they do bound the pressures requisite for a transition to Ice-VII (2.1 GPa) at room temperature [41] and exceed those requisite for a transition to Ice-VI (1.1 GPa). (It should be noted that the

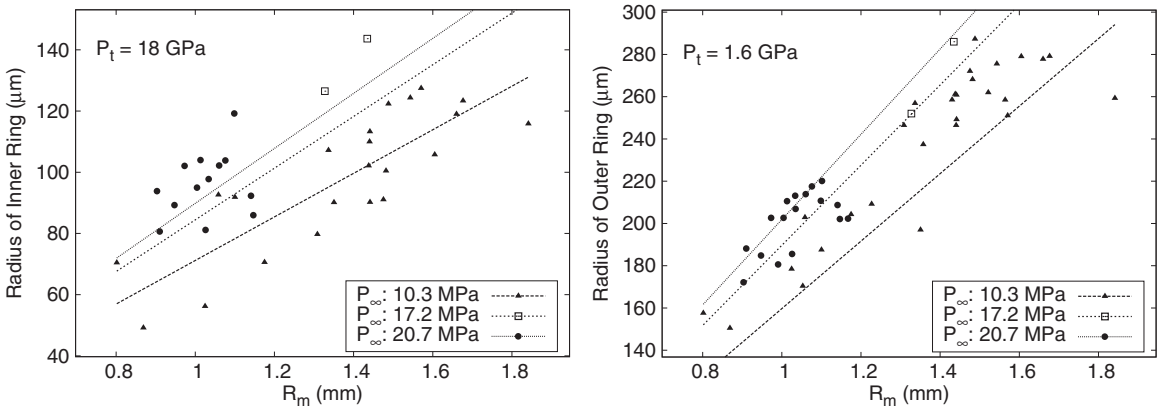

FIG. 12. Plots showing the dependence of the sizes of the inner (a) and outer (b) ring structures on the initial maximum bubble radius at the ambient pressures used in experiments. The dotted lines are the predicted radii [from Eq. (3)], where the pressures first exceed the value, P_t, as given in the plots. It can be seen for the boundary of the inner ring (a) that P_t is 18 GPa, and for the outer ring (b) that P_t is 1.6 GPa. The three sets of lines in each plot show the dependence of the structure size on the initial maximum bubble radius at different ambient pressures, where the values P_∞ of each line were chosen to correspond with the ambient pressures used in experiments.

transition pressures to these two phases of ice are consistent between the two species of water used in this study, and that there was no discernible difference observed experimentally in the functional relationship between the bubbles' maximum radii and the ring locations in H_2O compared to D_2O.) If we assume a crystalline transition, the presence of the observed rings at the 1.6 and 18 GPa pressure crossings can partly be explained by a time lag between when the pressure first crosses the threshold and when the actual phase transition begins [42]. As the bubble collapses it causes water to flow inwards towards it and the pressures around it to build up. In the event of a time lag between the pressure crossing and the phase change, the pressures in the fluid would continue to rise until the phase change arrested the liquid's motion. As a result the region of fluid above the transition pressure would have time to grow, both inwards and outwards, before the transition commenced. This process would ultimately come to a stop when the influx of fluid producing these high pressures was halted by the solid region, at which point the phase transition would stop and the bubble would collapse in the remaining fluid contained within the solid shell. As a phase transition process in the fluid would necessarily require energy, and the formation of a solid region around the bubble would impede the free motion of the inrushing fluid surrounding the collapsing bubble, such a process would likely alter the dynamics of the collapse, potentially producing observable outcomes in the process, which may have been manifested in the form of the unexpected similarity between the emission events observed in these experiments and those of Ramsey and Pitz.

Although calculations of the pressures in the fluid provide a foundation for the argument that the spheroids are the result of a crystalline transition in the fluid, observations of the dynamics of the objects suggest instead that they are the result of a transition to an amorphous or liquid state and that other considerations must be taken into account to describe them. Perhaps most importantly, pressurization in previous crystalline transition studies has primarily been quasistatic in nature and achieved through the use of anvil cells with crystal windows [43,44]. And while thermodynamic conditions present in the multiple shock wave compression studies differ from those in the quasistatic compression studies, in both studies contact with the windows provided heterogeneous nucleation sites for crystal growth and played a significant role in the observed transformations [14]. The ring structures observed in this study form in a region of liquid that experiences extreme pressurization rates, undergoes significant radial motion as the bubble evolves, and form in the absence of any apparent nucleation sites like windows to initiate heterogeneous growth. These factors must also be accounted for when considering a potential noncrystalline transition.

The velocity of the liquid at the locations of the observed rings at the time of the arrival of the pressure peak at each location can be derived via conservation of mass arguments in a fashion similar to that used to derive Eq. (3). Doing so, one finds that the fluid velocity u_{peak} at $r = r_{\text{peak}}$ is given by

$$u_{\text{peak}}^2 \approx \frac{2P_{\text{peak}}}{3\rho}, \tag{4}$$

where ρ is the liquid density. Surprisingly, the velocity of the liquid at r_{peak} does not depend explicitly on the minimum or maximum bubble radius or the location of the pressure maximum in the fluid and is instead only dependent on the peak Rayleigh pressure. For a peak pressure of 1.6 GPa, corresponding to the location of the outer boundary of the spheroidal object, we find the peak fluid velocity $u_{\text{peak}} \approx$ 1000 m/s; and for the inner boundary of the structure, where the peak pressure was calculated to be 18 GPa, the peak fluid velocity is $u_{\text{peak}} \approx 3500$ m/s. These fluid velocities at the observed locations of the spheroids' boundaries seem to favor arguments for a dynamic transition instead of a static or quasistatic one. Pressurization rates in the fluid at the locations of the ring structures are likewise extreme. It can be shown that, after the first crossing of the pressure maximum at the ring locations, pressures in the field within the boundaries of the rings continue to rise at rates up to or exceeding

1 GPa/ns. These pressurization rates also seem to favor a nonstatic transition, potentially in the form of a pressure analog to thermal hyperquenching, which has been shown previously to produce amorphous water ice [25].

Despite these pressurization rate and velocity results and the absence of windows, however, heterogeneous nucleation cannot be ruled out entirely as the formation of the spheroids could not be observed directly due to the obscured field of view resulting from the pressure field in the fluid refracting away light, and as processes known to occur within the bubbles themselves may generate products that could act as nucleation sites. While the velocity results suggest a dynamic transition, because we cannot see when the "freezing" occurs, we cannot say with certainty that it occurs while the radial liquid velocity is high. In addition to this, as bubbles collapse the gas within them heats up and ionizes [45,46], generating ionization products that may then escape the bubble entrained in Rayleigh-Taylor jets, or which may through contact at the bubble's surface act as nucleation sites for transitions. While it appears as though the ring structures form in the absence of these jets (Fig. 8), they cannot be ruled out as sources of heterogeneous nucleation.

An interesting consequence of the notion that these spheroidal objects are the result of a phase transition in the liquid, particularly to a crystalline phase which can impede the motion of the inrushing fluid, is that it suggests that there may be a fundamental, fluid-dependent limit to how much energy may be deposited to the core of a collapsing bubble from the field before processes in the field itself begin factoring into the energy equation. This could have important implications for determining what types of processes can occur within the cores of collapsing bubbles, as well as for determining what mechanisms are responsible for generating the light emissions observed. As has also been noted previously [13], such a transition in the fluid surrounding the collapsing bubble could help explain some of the anomalous features of sonoluminescence.

While the objects being the result of a crystalline transition would be an interesting result with important consequences, the notion that these objects may be the result of a transition to a liquid or amorphous state is potentially even more exciting. Particularly, while such a transition in water has not previously been observed at much above cryogenic temperatures, the conditions generated during these experiments have a number of novel features which could lead to such a result where others have not, including the high fluid velocities and pressurization rates in the field without the associated rise in temperatures normally accompanying such processes, as well as the absence of apparent heterogeneous nucleation sites for crystal growth. Although it would be interesting to assess the chemical and physical composition of the observed objects, the relatively short lifetime of these objects present a number of technical challenges toward making direct measurements. However, infrared imaging may provide a useful first step toward helping to determine the temperatures in the field during their generation and the processes underlying their formation. That such a transition may exist could have far reaching impacts in numerous fields of study where such a pressurization pathway has previously been unavailable, and the outcomes of which have remained unexplored. That is to say, the techniques used to generate the conditions in the fluid during these experiments are easily extensible to fluids other than water, and could provide insight into the types of processes or interactions that may occur under such conditions elsewhere in nature, or what types of materials or outcomes may be generated as a result.

V. CONCLUSION

The results of these experiments yielded a number of interesting and unexpected observations about the outcomes of the collapses of large single bubbles at high static pressures and raised a number of important questions which remain to be answered. Chief among them are what is the nature of the observed spheroids produced by the collapse events in this study? Observations of their behaviors and calculations of the pressures in the field at the locations where they were generated are strongly suggestive of a phase transition in the water. If that is the case, what kind of transition has taken place? The behaviors of the objects indicate that they are likely not the result of a transition to one of water's crystalline phases, but the temperatures at which they were generated are inconsistent with the generation of water's known amorphous phases. Further questions arise related to these objects about the other anomalous behaviors observed in these experiments. Are the light-emission events produced by collapsing bubbles affected by the generation of these objects? If so, does their presence help explain the lack of a more significant difference between the measurable quantities of the emission events observed in the present study and those observed previously, despite those in the present case being generated by the collapses of significantly more energetic bubbles? Further still, would this imply that there is a fundamental limit to how much energy may be deposited to the bubble's core before processes in the field began impeding the bubble's continued collapse, and if so what is this limit and how does it vary as a function of the host fluid?

To answer these questions and others, future work may take a number of different directions. Perhaps the simplest, and potentially most impactful, would be to repeat the current experiments in a fluid other than water. If the objects observed truly are the result of a phase transition in water, such a transition might be observable in other fluids as well and might produce longer lived and easier to study transition products. Even if such a transition were unique to water, this would still go a long way in answering questions about the light emission events. For instance, in a fluid in which these objects were not observed to form, light emissions produced by the collapse of more energetic bubbles might scale as expected and produce larger and/or longer lived events. Or if such a transition were not unique to water, deviations from expectations in the emission products versus collapse energy curve could be used as an indicator for when such a transition occurs in other fluids. Additional studies might also be carried out in water at higher ambient pressures, or which can generate larger bubbles to test whether the scaling relationships observed here hold as collapses become even more energetic. Further, owing to limitations of the equipment used in this study, the decay of the objects could not be observed before bubbles generated in the subsequent acoustic cycles tore them apart. A system that could suppress or eliminate the growth of bubbles at later time points could allow the evolution of these objects over

their unimpinged-upon lifetimes to be studied and provide additional information about what they are. Whatever directions future work might take, the questions raised by this study will take significantly more work to understand and explain.

ACKNOWLEDGMENT

This work was funded by Impulse Devices, Inc., Grass Valley, CA.

[1] D. F. Gaitan, L. A. Crum, C. C. Church, and R. A. Roy, Sonoluminescence and bubble dynamics for a single, stable, cavitation bubble, J. Acoust. Soc. Am. **91**, 3166 (1992).

[2] D. F. Gaitan, R. A. Tessien, R. A. Hiller, J. Gutierrez, C. Scott, H. Tardif, B. Callahan, T. J. Matula, L. A. Crum, R. G. Holt, C. C. Church, and J. L. Raymond, Transient cavitation in high-quality-factor resonators at high static pressures, J. Acoust. Soc. Am. **127**, 3456 (2010).

[3] J. R. Sukovich, A. Sampathkumar, P. A. Anderson, R. G. Holt, Y. A. Pishchalnikov, and D. F. Gaitan, Temporally and spatially resolved imaging of laser-nucleated bubble cloud sonoluminescence, Phys. Rev. E **85**, 056605 (2012).

[4] C. C. Church, D. F. Gaitan, Y. A. Pishchalnikov, and T. J. Matula, The effects of hydrostatic pressure on conditions in and near a collapsing cavitation bubble, J. Acoust. Soc. Am. **129**, 2620 (2011).

[5] D. F. Gaitan, Theory and current experimental data regarding the possibility of acoustic inertial confinement fusion, in *Proceedings of the International Symposium on Sustainability in Acoustics, ISSA* (August, Auckland, New Zealand, 2010).

[6] B. Gompf, R. Günther, G. Nick, R. Pecha, and W. Eisenmenger, Resolving Sonoluminescence Pulse Width with Time-Correlated Single Photon Counting, Phys. Rev. Lett. **79**, 1405 (1997).

[7] M. J. Moran, R. E. Haigh, M. E. Lowry, D. R. Sweider, G. R. Abel, J. T. Carlson, S. D. Lewia, A. A. Atchley, D. F. Gaitan, and X. K. Maruyama, Direct observations of single bubble sonoluminescence pulses, Nucl. Instr. Methods Phys. Res. B: Beam Interact. Mater. Atoms **96**, 651 (1995).

[8] M. C. Ramsey and R. W. Pitz, Energetic Cavitation Collapse Generates 3.2 mbar Plasma with a 1.4 J Driver, Phys. Rev. Lett. **110**, 154301 (2013).

[9] L. Rayleigh, On the pressure developed in a liquid during the collapse of a spherical cavity, Philos. Mag. **34**, 94 (1917).

[10] A. H. Harvey, A. P. Peskin, and A. K. Sanford, NIST, ASTME–IAPSW Standard Reference Database 10 (1996).

[11] E. Sanz, C. Vega, J. L. F. Abascal, and L. G. MacDowell, Phase Diagram of Water from Computer Simulation, Phys. Rev. Lett. **92**, 255701 (2004).

[12] H. G. Flynn, Collapse of a transient cavity in a compressible liquid. part I. an approximate solution, Technical report, DTIC document (1957).

[13] R. Hickling, Transient, High-Pressure Solidification Associated with Cavitation in Water, Phys. Rev. Lett. **73**, 2853 (1994).

[14] D. H. Dolan and Y. M. Gupta, Nanosecond Freezing of Water Under Multiple Shock Wave Compression; Optical Transition and Imaging Measurements, J. Chem. Phys. **121**, 9050 (2004).

[15] K. Ohsaka and E. H. Trinh, Dynamic nucleation of ice induced by a single stable cavitation bubble, Appl. Phys. Lett. **73**, 129 (1998).

[16] B. Lindinger, R. Mettin, R. Chow, and W. Lauterborn, Ice Crystallization Induced by Optical Breakdown, Phys. Rev. Lett. **99**, 045701 (2007).

[17] R. K. Bhaskaracharya, S. Kentish, and M. Ashokkumar, Selected applications of ultrasonics in food processing, Food Eng. Rev. **1**, 31 (2009).

[18] O. Mishima and H. E. Stanley, The relationship between liquid, supercooled and glassy water, Nature **396**, 329 (1998).

[19] H. Patashnick, G. Rupprecht, and D. W. Schuerman, Energy source for comet outbursts, Nature **250**, 313 (1974).

[20] R. Smoluchowski, Adsorption and mobility on amorphous surfaces: Application to astrophysics, J. Phys. Chem. **87**, 4229 (1983).

[21] E. Mayer and R. Pletzer, Astrophysical implications of amorphous ice—a microporous solid, Nature **432**, 731 (1986).

[22] P. Jenniskens and D. F. Blake, Structural transitions in amorphous water ice and astrophysical implications, Science **265**, 753 (1994).

[23] O. Mishima, L. D. Calvert, and E. Whalley, 'Melting Ice' I at 77 K and 10 kbar: A new method of making amorphous solids, Nature **310**, 393 (1984).

[24] R. J. Hemley, L. C. Chen, and H. K. Mao, New transformations between crystalline and amorphous ice, Nature **338**, 638 (1989).

[25] V. Velikov, S. Borick, and C. A. Angell, The glass transition of water, based on hyperquenching experiments, Science **294**, 2335 (2001).

[26] R. S. Smith, N. G. Petrik, G. A. Kimmel, and B. D. Kay, Thermal and nonthermal physiochemical processes in nanoscale films of amorphous solid water, Acc. Chem. Res. **45**, 33 (2012).

[27] R. C. Dougherty, The PVT surface of water: Critical phenomena near 0.195 GPa, 182 K, Chem. Phys. **298**, 307 (2004).

[28] J. R. Sukovich, A. Sampathkumar, and R. G. Holt, Pressure dependence of laser-induced dielectric breakdown in water, IEEE J. Quant. Electron. **47**, 1297 (2011).

[29] Y. A. Pishchalnikov, J. Gutierrez, W. W. Dunbar, and R. W. Philpott, Intense cavitation at extreme static pressure, Ultrasonics **65**, 380 (2016).

[30] P. A. Anderson, A. Sampathkumar, T. W. Murray, D. F. Gaitan, and R. G. Holt, Optical nucleation of bubble clouds in a high pressure spherical resonator, J. Acoust. Soc. Am. **130**, 3389 (2011).

[31] R. Fernandez-Prini and R. Dooley, Release on the refractive index of ordinary water substance as a function of wavelength, temperature and pressure, *International Association for the Properties of Water and Steam* (Erlangen, Germany, 1997), pp. 1–7.

[32] J. Holzfuss, M. Rüggeberg, and A. Billo, Shock Wave Emissions of a Sonoluminescing Bubble, Phys. Rev. Lett. **81**, 5434 (1998).

[33] G. Taylor, The instability of liquid surfaces when accelerated in a direction perpendicular to their planes, Proc. Roy. Soc. London A. Math. Phys. Sci. **201**, 192 (1950).

[34] W. Lauterborn and H. Bolle, Experimental investigations of cavitation-bubble collapse in the neighbourhood of a solid boundary, J. Fluid Mech. **72**, 391 (1975).

[35] C.-D. Ohl, T. Kurz, R. Geisler, O. Lindau, and W. Lauterborn, Bubble dynamics, shock waves and sonoluminescence, Philos.

Trans. Roy. Soc. London A: Math. Phys. Eng. Sci. **357**, 269 (1999).

[36] K. Yasui, Effect of liquid temperature on sonoluminescence, Phys. Rev. E **64**, 016310 (2001).

[37] K. Yasui, Temperature in multibubble sonoluminescence, J. Chem. Phys. **115**, 2893 (2001).

[38] K. Yasui, T. Tuziuti, T. Kozuka, A. Towata, and Y. Iida, Relationship between the bubble temperature and main oxidant created inside an air bubble under ultrasound, J. Chem. Phys. **127**, 154502 (2007).

[39] K. Yasui, T. Tuziuti, J. Lee, T. Kozuka, A. Towata, and Y. Iida, The range of ambient radius for an active bubble in sonoluminescence and sonochemical reactions, J. Chem. Phys. **128**, 184705 (2008).

[40] J. R. Sukovich, On the origins and outcomes of laser-nucleated bubble collapse events at high ambient pressures, Ph.D. thesis, Boston University (2013).

[41] V. P. Dmitriev, S. B. Rochal, and P. Toledano, Theory of Ice Structures, Phys. Rev. Lett. **71**, 553 (1993).

[42] M. Bastea, S. Bastea, J. E. Reaugh, and D. B. Reisman, Freezing kinetics in overcompressed water, Phys. Rev. B **75**, 172104 (2007).

[43] R. J. Hemley, A. P. Jephcoat, H. K. Mao, C. S. Zha, L. W. Finger, and D. E. Cox, Static compression of H_2O-ice to 128 GPa (1.28Mbar), Nature **330**, 737 (1987).

[44] H. Shimizu, T. Nabetani, T. Nishiba, and S. Sasaki, High-pressure elastic properties of the VI and VII phase of ice in dense H_2O and D_2O, Phys. Rev. B **53**, 6107 (1996).

[45] D. J. Flannigan and K. S. Suslick, Plasma formation and temperature measurement during single-bubble cavitation, Nature **434**, 52 (2005).

[46] B. Kappus, S. Khalid, A. Chakravarty, and S. Putterman, Phase Transition to an Opaque Plasma in a Sonoluminescing Bubble, Phys. Rev. Lett. **106**, 234302 (2011).